Tautomerization of Single Asymmetric Oxahemiporphycene Molecules on Cu(111)

Simon Jaekel[1,2], Emile Durant[3], Monika Schied[1], Mats Persson[3], Jakub Ostapko[4], Michał Kijak[4], Jacek Waluk[4,5], and Leonhard Grill[1*]

[1] Department of Physical Chemistry, University of Graz, Heinrichstraße 28, Graz, Austria

[2] Chair for Physical Chemistry II, Friedrich-Alexander-University Erlangen-Nürnberg, Egerlandstraße 3, Erlangen, Germany

[3] Surface Science Research Centre, Department of Chemistry, University of Liverpool, Liverpool L69 3BX, UK

[4] Institute of Physical Chemistry, Polish Academy of Sciences, Kasprzaka 44/52, 01-224 Warsaw, Poland

[5] Faculty of Mathematics and Science, Cardinal Stefan Wyszyński University, Dewajtis 5, 01-815 Warsaw, Poland

* corresponding author: leonhard.grill@uni-graz.at

Contents

1. Preferential adsorption at step edges

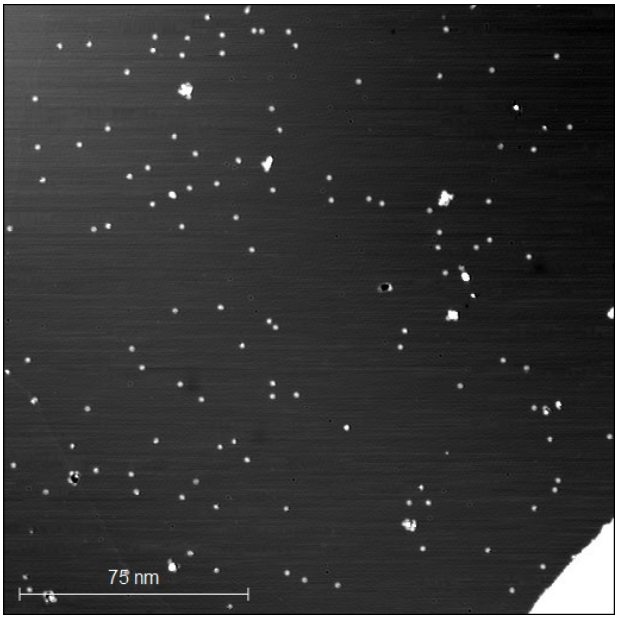

Figure S1: STM topography image (200×200 nm², 500 mV, 50 pA) of O-HPc molecules on a terrace of the Cu(111) surface. Single molecules are visible as bright dots.

As shown in Figure S1, a comparatively large number of single O-HPc molecules can be found on the terraces of images taken at surface area with few step edges. In contrast, no coverage on the terraces is visible in Figure S2, which shows a section of the same sample, as depicted in Figure S1, but with a higher number of step edges within the scan frame. From this it can be concluded that the molecules preferentially adsorb at step edges and are only found on the terraces once all step edge sites have been covered.

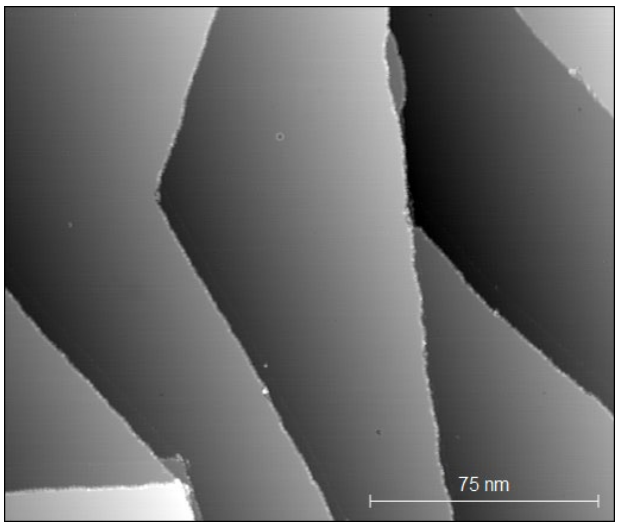

Figure S2: STM topography images (200×169 nm², 500 mV, 50 pA) of O-HPc molecules on a stepped area of the Cu(111) surface showing only decoration of the step edges.

2. Orientation of the Cu(111) crystal

To gain information regarding the orientation of the adsorbed molecules with respect to the directions of the crystal, atomically resolved images were acquired at increased tunneling current, as shown in Figure S3. The main symmetry axes derived from the scan were used to evaluate the alignment of molecules in larger images.

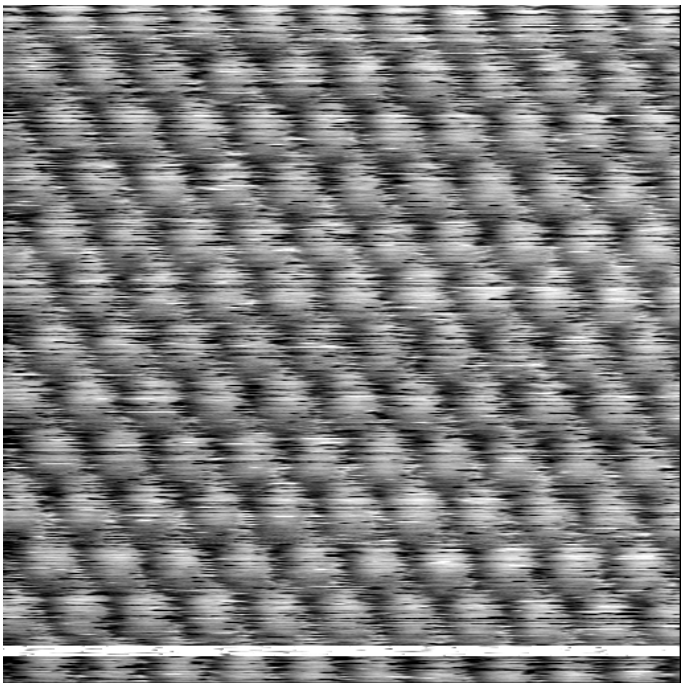

Figure S3: Atomically resolved STM image (2.55×2.55 nm^2, 200 mV, 1.4 nA) of the Cu(111) surface.

3. Imaging of copper atoms and oxahemiporphycene in the same image

Attempting to image the copper surface with the adsorbed O-HPc molecules in the same image usually leads to either a highly distorted appearance of the molecules or a lateral displacement of the molecules through the tip-molecule interaction. This is caused by the stronger interaction force at lower tip-sample distance at the require imaging conditions. To avoid this effect, the current setpoint during the acquisition of Figure 1d was adjusted during image acquisition. The areas showing the copper atoms were acquired at 10 mV bias and 9 nA tunneling current. To image the molecule the current set point was reduced to 25 pA. The setpoint adjustments were made gradually to avoid instabilities of the feedback loop near the horizontal scan lines 120 and 395 (counting from the start of the scan at the top). The regions with different tunneling current have distinct apparent heights, making it necessary to apply different color scales in each of them to allow sufficient visibility of all features. As a consequence, pixels with the same brightness over the molecule and the copper atoms do not correspond to the same apparent height.

4. Deprotonation using the tunneling current

The tunneling current is plotted in Fig. S4 as a function of the time during a voltage pulse with increased bias voltage at the position used for the switching experiments. The deprotonation of the molecule is concluded from the changed topography of the molecule and the absence of bistability of the conductance during consequent switching attempts of the same molecule.

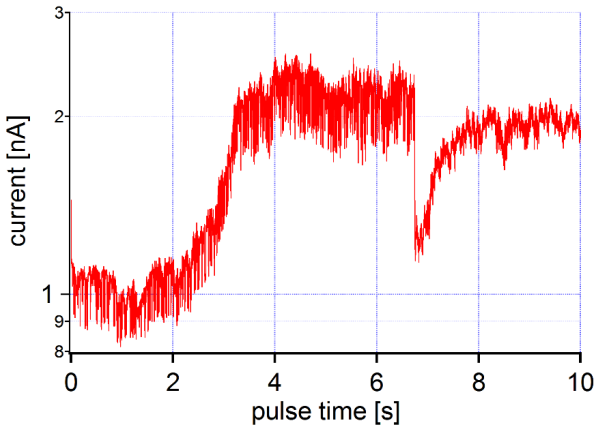

Figure S4: I(t) graph during a voltage pulse with 2.0 V used for deprotonation of the O-HPc molecule. Initial noise corresponds to rapid cis ↔ trans switching with rates near the resolution limit. The steep drop after more than 6 s marks the removal of the iminic hydrogen. The S-shaped background is an artifact of our measurement system, which appeared at high tunneling current values.

5. Automated fitting of the switching data

To speed up the evaluation of the switching data, we used the algorithm developed by Yuzhelevski *et al.* [1] and implemented it in Python. It fits the histogram of the tunneling current with two gaussian distributions, as shown in Figure S5, to identify the conductance levels. Then, it seeks immediate jumps between these two populations and marks them as a switching event. From this information it produces a two-level fit to the acquired data in the shape of a line that jumps between two discrete levels, as shown in Figure S6. Resulting from this fit the average values (and their standard deviations) of the tunneling current in the lower and higher conductance state, the population of each conductance state, and the number of switching events between the two levels are determined. The sum of the dwelling time in each state is calculated from the histogram populations. Combined with the number of switching events, it can be used to calculate the average switching times $\langle T \rangle$ in the following way:

$$\langle T \rangle = \frac{T \cdot P}{N}$$

where T is the summed duration of all switching pulses, and P is the normalized population of either conductance state. For a first-order switching process where the number of switching events N(t) in a time frame from t to $t + \delta t$ can be described in the following form

$$N(t) = N_0 \cdot exp(-R \cdot t)$$

with R being the switching rate. It is possible to directly calculate R from $1/\langle T \rangle$, as used in the main text, for this type of switching law, because:

$$\langle T \rangle = \lim_{N \to \infty} \frac{\sum T_i}{N} = \frac{\int_0^\infty t \cdot N(t) dt}{\int_0^\infty N(t) dt} = \frac{1}{R}$$

The exponential decay of the number of switching event with time was confirmed for a single (bias voltage, tunneling current) data point through timing of individual events by hand. After this confirmation, the faster algorithmic evaluation was employed only.

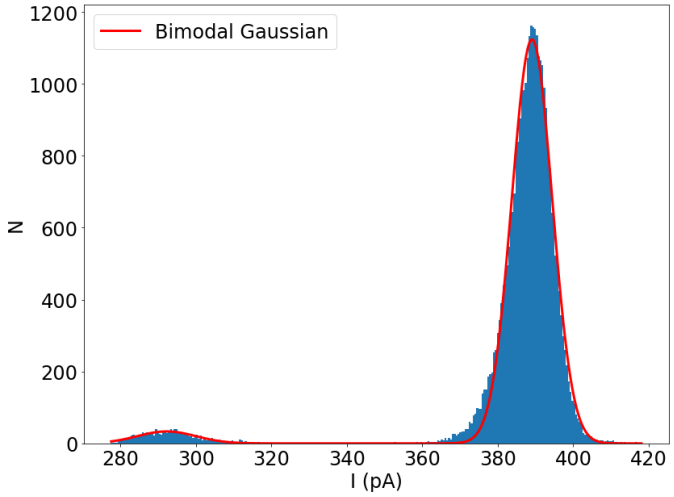

Figure S5: Histogram of the data shown in Fig. S4 with the fitted populations shown in red and the experimental data shown in blue.

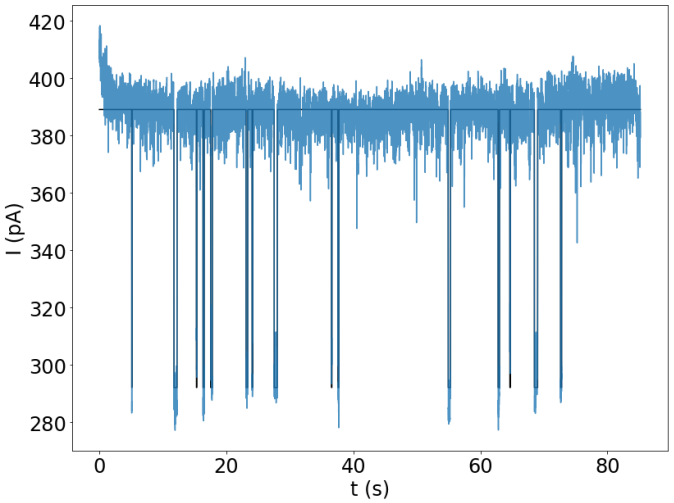

Figure S6: Example output of the fitting algorithm to a conductance tunneling current trace acquired with a bias voltage of -1.4 V.

6. Switching traces during measurements with variable tip position

During the acquisition of the position dependent switching rates shown in Figure 4b, it was noticed that the noise level during individual switching traces was also dependent on the location of the tip over the molecule. The increased noise amplitude, exemplarily shown in Figure S7, cannot be attributed to instabilities of the tip or detection apparatus, because only time spectra acquired over some pixels exhibited them, while others showed the usual noise levels (such as shown in Figure 3a). The presence or absence of this increased signal noise was reproducible over specific spectroscopic locations. As long as switching events were still visible to the naked eye, as seen in Figure S7, spectra were used for the evaluation of the switching activity.

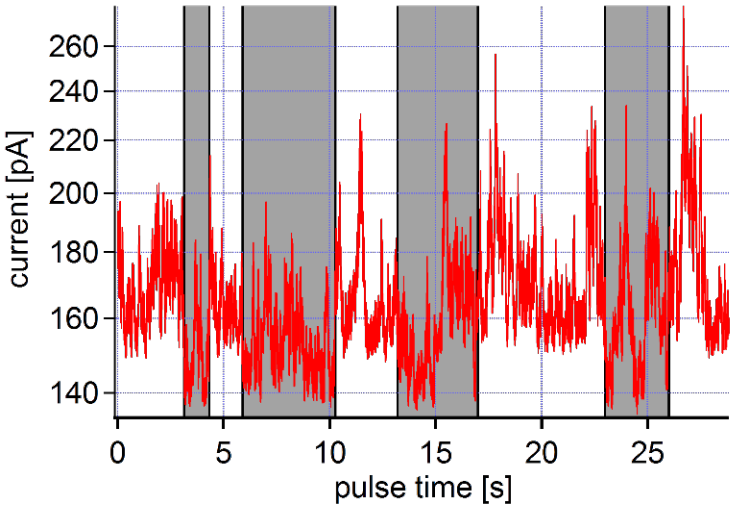

Figure S7: Example tunneling current spectrum acquired at a pixel near, but off the bottom pyrrole ring. It can be seen that the baseline of the current shifts between two levels around 145 pA and around 155 pA, respectively (the low conductance state is marked in grey, the probable transitions are indicated by black lines). However, the noise amplitude is larger than the separation of the levels and its shape is highly non-gaussian. Eight back-and-forth switching events are visible.

7. Calculated gas phase structures

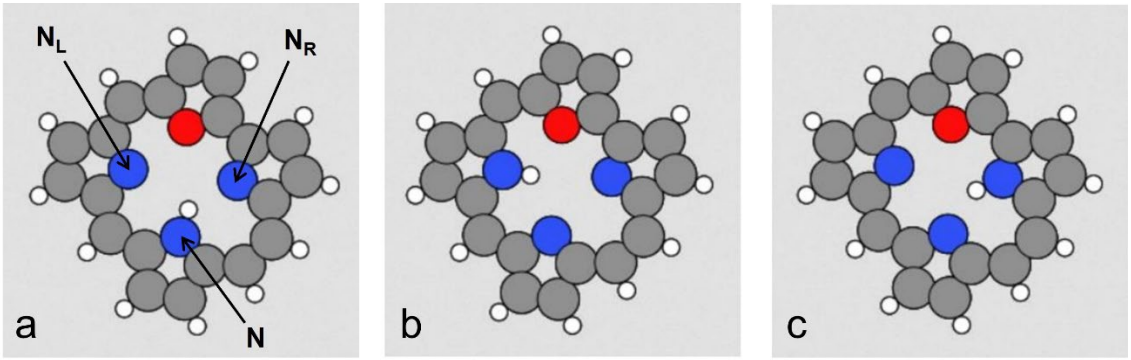

Figure S8: Top views of the (a) trans, (b) cis$_L$ and (c) cis$_R$ tautomers of O-HPc. The different nitrogen atoms N, N$_L$ and N$_R$ are indicated in (a).

8. Interatomic distances for the adsorbed tautomers of O-HPc on Cu(111)

Here, we examine the geometries of the adsorbed tautomers on the Cu(111) surface. Two equilibrium structures were identified for each adsorbed tautomer, which differ only by the position of the O atom relative to the *hollow-fcc* and *hollow-hcp* sites of the Cu(111) surface. For a given tautomer, the adsorption energies of the two equilibrium structures show only minor differences which are not significant for the proton atom transfer. Therefore, it is sufficient to present results only for one of the structures for each tautomer, where the O atom is close to the *hollow-fcc* site. These structures are shown in Fig. S9. The results for the other structures where the O atoms are close to the *hollow-hcp* site are presented elsewhere [2].

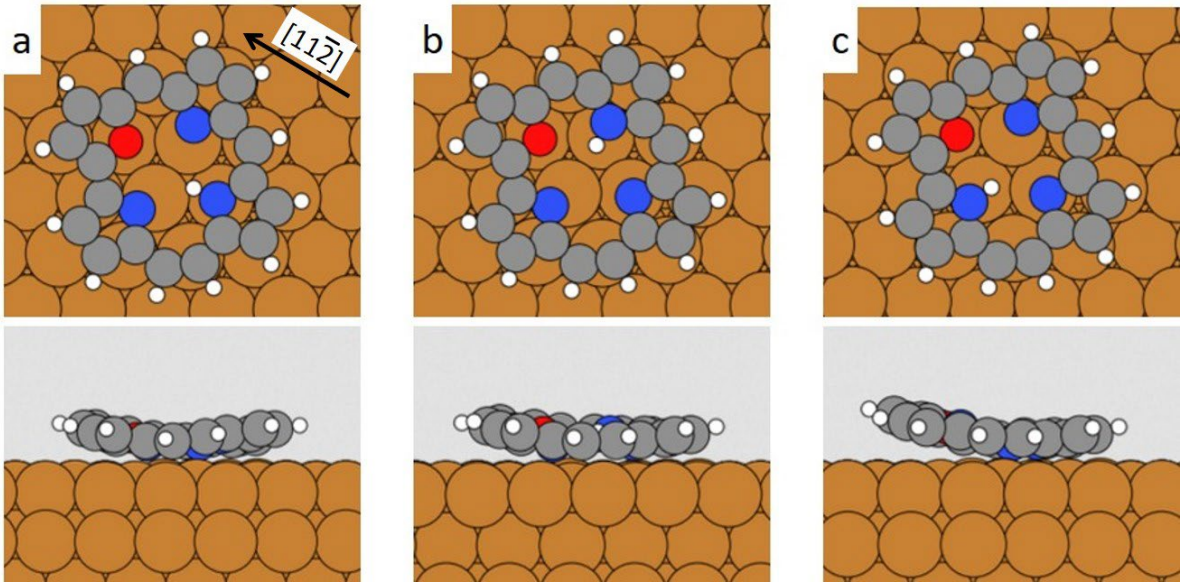

Figure S9: Top and side views of the adsorbed (a) trans, (b) cis$_L$ and (c) cis$_R$ tautomers in the hollow-fcc site on the Cu(111) surface in the upper and lower panel, respectively.

As shown in Fig, S9, all adsorbed tautomers are oriented along the $[11\bar{2}]$ direction (indicated in Fig. S9a). Another common feature of all the adsorbed tautomers is the bending of the molecule, which is driven by the bonding of the lone pairs of the imine N atoms to surface Cu atoms. The N-Cu distances for imine N atoms are about 2.02 – 2.12 Å, whereas the corresponding distances for the amine N atoms are approximately 0.3 – 0.7 Å larger and are close to the O-Cu distances. Compared to the N-N distances in the gas phase, there are significant differences in the N-N distances except for the N_L-N_R distances, the latter only showing small changes. In particular, the difference between the N-N_L and the N-N_R distances are significantly reduced from 0.33 Å to 0.03 Å and the order of these distances between the tautomers are reversed. All these distances are shown in Tables S1 and S2.

Tautomer	N-Cu (Å)	N_L-Cu (Å)	N_R-Cu (Å)	O-Cu (Å)
trans	2.43	2.08	2.11	2.41
cis$_R$	2.07	2.05	2.83	2.74
cis$_L$	2.07	2.63	2.06	2.60

Table S1: Calculated nearest-neighbour N-Cu and O-Cu interatomic distances for the three tautomers of O-HPc in the hollow-fcc site on Cu(111). The labelling of the N atoms is defined as in Fig. S8.

Tautomer	N-N_L (Å)	N-N_R (Å)	N_L-N_R (Å)
trans	3.08	3.18	3.98
cis$_R$	3.17	3.14	3.95
cis$_L$	3.10	3.27	4.02

Table S2: Calculated N-N interatomic distances for the three tautomers of O-HPc in the hollow-fcc site on Cu(111). The labelling of the N atoms is defined as in Fig. S8.

9. Calculated structure of the three tautomers on Cu(111)

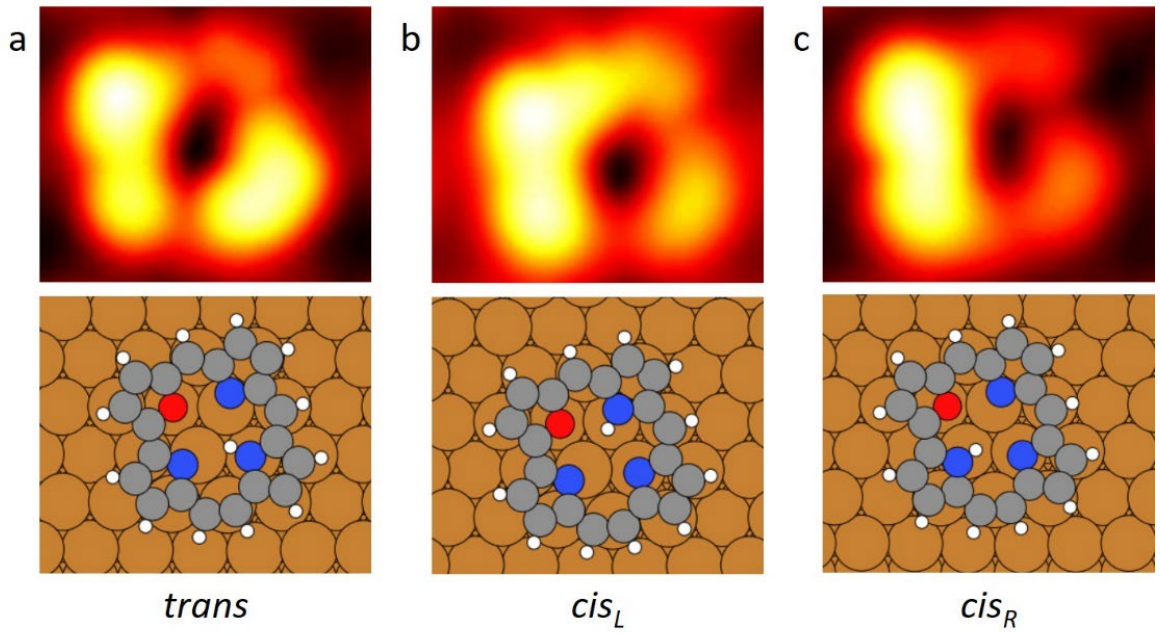

Figure S10: Simulated topographical STM images of (a) trans, (b) cis$_L$ and (c) cis$_R$ tautomers in the hollow-fcc site on the Cu(111) surface. The lower panel shows the surface and the chemical structures, corresponding to the simulated images in the upper panel: Cu atoms (brown), H (white), C (grey), N (blue), and O (red). The average tip-surfaces heights are (a) 7.4 Å, (b) 7.8 Å and (c) 8.0 Å.

10. Dehydrogenated O-HPc adsorbed on Cu(111)

Here, we present the calculated geometric structure and dehydrogenation energies of O-HPc both in the gas phase and adsorbed on the surface. As for the tautomers of O-HPc in the gas phase, the dehydrogenated O-HPc is also planar in the gas phase. There are some distortions of the macrocycle upon dehydrogenation in the gas phase as shown by the shortening of the N-N interatomic distance by about 0.2 Å compared to the *trans* tautomer distortion.

	ΔE (eV)	**N-N$_L$ (Å)**	**N-N$_R$ (Å)**	**N$_L$-N$_R$ (Å)**
Gas phase	3.02	3.08	3.01	4.01
Adsorbed	0.66	3.12	3.27	4.00

Table S3: Calculated dehydrogenation energies ΔE and N-N interatomic distances for the dehydrogenated O-HPc in the gas-phase. The labelling of the N atoms is defined as in Fig. S8.

The dehydrogenated O-HPc is also bent upon adsorption as shown in Fig. S11, but in this case there are no amine N atoms and the N-Cu distances are the same as for the imine N atoms of the adsorbed tautomers (see Tables S1 and S4).

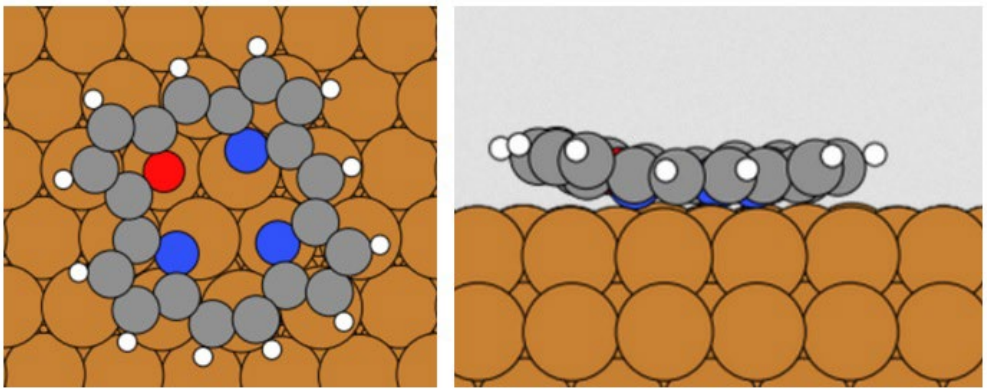

Figure S11: Top and side views of the dehydrogenated O-HPc adsorbed in the hollow-fcc site on Cu(111).

N-Cu (Å)	N_L-Cu (Å)	N_R-Cu (Å)	O-Cu (Å)
2.02	2.03	2.04	2.38

Table S4: Calculated nearest-neighbour N-Cu and O-Cu interatomic distances for the dehydrogenated O-HPc adsorbed in the hollow-fcc site on Cu(111). The labelling of the N atoms is defined as in Fig. S8.

The dehydrogenation energy ΔE in the gas phase and on the surface in Table S3 is defined with respect to the *trans* tautomer as

$$\Delta E[\text{gas phase}] = E[\text{OPc}] + \frac{1}{2}E[\text{H}_2] - E[\text{O-HPc}],$$

and

$$\Delta E[\text{surface}] = E[\text{OPc/Cu(111)}] + \frac{1}{2}E[\text{H}_2] - E[\text{O-HPc/Cu(111)}].$$

Here $E[\text{OPc}]$, $E[\text{OPc/Cu(111)}]$, $E[\text{H}_2]$, $E[\text{O-HPc}]$ and $E[\text{O-HPc/Cu(111)}]$ are the total energies of the dehydrogenated O-HPc in the gas phase and on the surface, the hydrogen molecule in the gas phase and the *trans* tautomer of O-HPc in the gas phase and on the surface. As shown in Table S3 there is a large reduction of the dehydrogenation energy upon adsorption.

11. Minimum energy paths

Here we present the calculated minimum energy paths (MEPs) for proton transfers between the tautomers of O-HPc on Cu(111) both in the gas phase and adsorbed on the surface. They were obtained using the climbing image – nudged elastic band (CI-NEB) method and are shown in Fig. S12. In the gas phased, only an indirect MEP for the *cis*$_L$ ↔ *cis*$_R$ tautomerization via the *trans* tautomer was found in the CI-NEB calculations. The participation of the substrate atoms in the tautomerization was found to be negligible since the path lengths for the tautomerizations in Fig. S12 are very close to the pathlengths including only the adsorbate atoms as shown by the result for D_{mol} in Table 3.

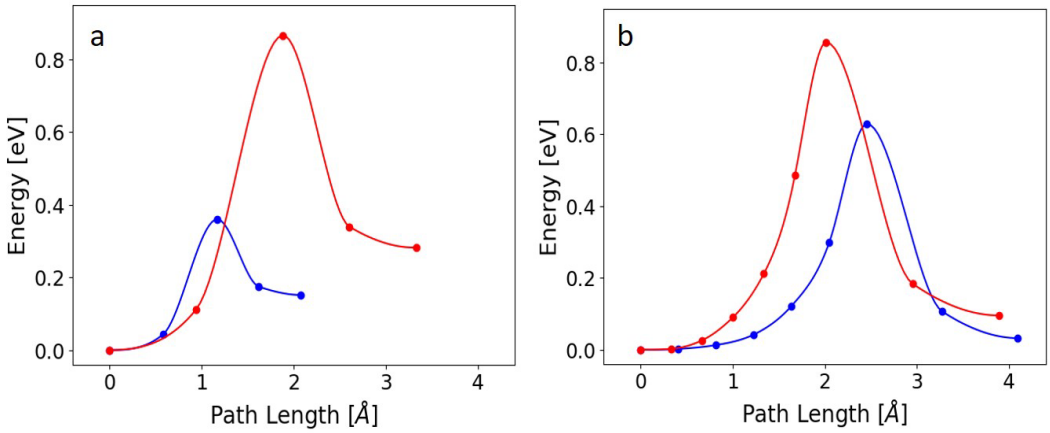

Fig. S12: Calculated MEPs from trans to left-cis (red) and right-cis (blue) tautomers of the O-HPc molecule in the gas phase (a) and adsorbed on the surface (b). The images along the MEP are indicated by solid circles. The path lengths were calculated from the distances between the images in configuration space including all atoms.

12. Vibrational energies and zero-point energy corrections

The N-H stretch vibrational energy was calculated in the harmonic approximation, where the dynamical matrix was obtained from calculated forces using central differences. All atoms except the inner H atom were kept fixed. The resulting N-H stretch vibration energies were 398, 472 and 407 meV for the *trans*, *right* and *left* tautomer, respectively. The changes in zero-point-energies (ZPEs) between the *trans* tautomer and the transition structures were estimated by calculating the corresponding changes of vibrational energies of the H atom while keeping all the remaining atoms fixed. The presence of a single mode with an imaginary vibrational energy indicates that the calculated saddle points in the CI-NEB calculations are proper transition structures.

13. Synthesis

All solvents and chemicals were of reagent grade quality, obtained commercially from SigmaAldrich, POCH, ABCR, ARMAR and used without further purification. NMR spectra were measured with a Varian Mercury 400 MHz and Varian VNMRS 600 MHz instruments. MS EI and ESI were registered using GCT Premier (Waters) and 4000 Q-TRAP (Applied Biosystems) spectrometers, respectively. Column chromatography was performed using Silica Gel 60 0.04-0.063 mm (Roth).

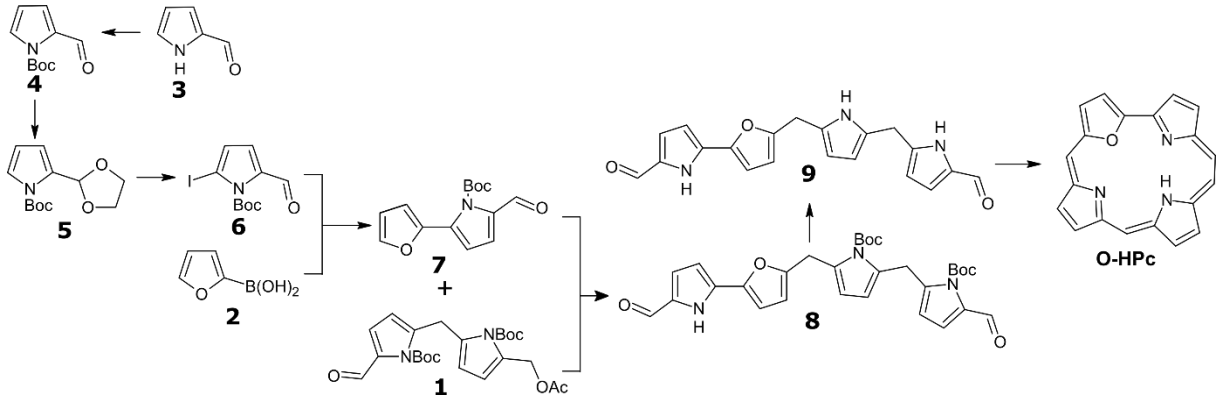

Figure S13: Scheme of 22-oxahemiporphycene synthesis and compounds numbering.

5-formyl-5'-hydroxymethyl-N,N'-di-*t*-butoxycarbonyl-2,2'-bipyrrylmethane (1) was synthesized according to the previously reported procedure [3]: ^{1}H NMR (500 MHz, $CDCl_3$) δ 9.98 (s, 1H), 7.03 (d, J=3.75Hz, 1H), 6.12 (d, J=3.25, 1H), 5.81 (d, J=3.25, 1H), 5.79 (d, J=3.75, 1H), 4.61 (s, 2H), 4.31 (s, 2H), 3.48 (s, br, 1H), 1.56 (s, 9H), 1.45 (s, 9H)

2-furanylboronic acid (2). The solution of furane was prepared by dissolving freshly distilled furane (5.1 g, 74.92 mmol) in dry THF (50 mL) under Ar atmosphere. The solution was cooled to 0°C by ice bath and *n*-BuLi solution was added (30 mL, 78.6 mmol, 2.5 M) dropwise, keeping the solution temperature below 5°C. Upon completing the addition of *n*-BuLi, the solution temperature was kept at 0°C for 30 min and then the ice bath was replaced by dry ice-acetone bath, reducing the temperature to -78°C. At this temperature trimethyl borate (16.5 mL, 150 mmol) was added by fast injection. Directly after addition of trimethyl borate the cooling bath was removed, and the mixture was allowed to reach room temperature. The mixture was then poured into ammonium chloride solution and stirred for 5 min. Next, the mixture was extracted with ethyl acetate. The organic phase was separated and washed with NaOH solution (10%). The water phase was then acidified by addition of HCl and extracted with ethyl acetate. The organic phase was separated, washed with brine, and dried over $MgSO_4$. Solvent evaporation resulted in the formation of solid material, which was washed with pentane and filtered. The product was obtained as a white solid powder with 25% yield (2.13 g; 19.03 mmol). ^{1}H NMR (500 MHz, DMSO-d_6) δ 7.81 (dd, J = 1.5, 0.5 Hz, 1H), 7.07 (dd, J = 3.0, 0.5 Hz, 1H), 6.48 (dd, J = 3.5, 2.0 Hz, 1H). The ^{1}H NMR spectrum agrees with literature data [4].

2-formylpyrrole (3) To the solution of pyrrole (10 mL, 144.3 mmol) in DMF (150 mL) cooled to 0ºC, $POCl_3$ (16 mL, 173.2 mmol) was added dropwise. The mixture was then stirred at 0ºC for 30 min and, after that time, was allowed to reach room temperature. The mixture was poured into Na_2CO_3 solution (60 g in 500 mL H_2O). The product was extracted with ethyl acetate. The organic phase was washed with water and brine. Next, the organic phase was separated and dried over $MgSO_4$. Evaporation of the solvent gave the product as a brown oil, which crystallized overnight. The product was re-crystallized by dissolving the material in hot hexane, separation from undissolved residue, and cooling the solution. The product was obtained as a colorless crystalline solid (14.44 g, 140 mmol) with 97% yield. ^{1}H NMR ($CDCl_3$, 300 MHz) δ 10.29 (s, 1H), 7.41 (m, 1H), 7.14 (m, 1H), 6.24 (m, 1H), 1.61 (s, 9H). The ^{1}H NMR spectrum agrees with literature data [5].

N-*t*-butoxycarbonyl-2-formylpyrrole (4) To 2-formylpyrrole **2** (5.0 g, 52.5 mmol) dissolved in THF (100 mL) triethylamine (30 mL, 0.2 mol), DMAP 4-dimethylaminopyridine, (1.28 g, 10 mmol) and di-*t*-butyl dicarbonate $(Boc)_2O$ (14.5 g, 63.1 mmol) were added. The mixture was stirred at room temperature for 1 hour. After that time H_2O (20 mL) was added and the mixture was stirred for 30 min. Next, the organic solvent was evaporated under reduced pressure and the product was extracted by diethyl ether. The organic phase was then filtrated through silica pad and the product was eluted by diethyl ether. The filtrate was evaporated giving the product as a pale-yellow oil (10.2 g, 52.5 mmol) with quantitative yield. ^{1}H NMR ($CDCl_3$, 300 MHz) δ 10.29 (s, 1H), 7.41 (m, 1H), 7.14 (m, 1H), 6.24 (m, 1H), 1.61 (s, 9H). The ^{1}H NMR spectrum agrees with literature data [6].

N-*t*-butoxycarbonyl-2-formylpyrrole acetal (5) N-*t*-butoxycarbonyl-2-formylpyrrole **3** (8.0 g, 41 mmol) was dissolved in benzene (150 mL). Ethylene glycol (8 mL, 143 mmol) and a few milligrams of *p*-toluenesulfonic acid were added. The mixture was brought to the boiling point and the benzene/water azeotrope was collected by Dean-Stark apparatus. The reaction was monitored by TLC (ethyl acetate:hexane 1:10, SiO_2). Upon total substate conversion, ethyl acetate (200 mL) was added, and the organic phase was washed with water solution of sodium carbonate. The product was isolated by column chromatography (ethyl acetate:hexane 1:10, SiO_2) as a deep-yellow oil (7.8 g, 32.8 mmol) with 80% yield. ^{1}H NMR δ 1.60 (s, 9H), 3.97−4.06 (m, 4H), 6.13 (t, J = 3.3 Hz, 1H), 6.41−6.43 (m, 1H), 6.45 (s, 1H), 7.24 (dd, J = 3.3 Hz, J = 1.8 Hz, 1H). The ^{1}H NMR spectrum agrees with literature data [7].

5-iodo-2-formyl-N-*t*-butoxycarbonylpyrrole (6) To the solution of 2,2,6,6-tetramethylpiperidine (12.6 mL, 71.05 mmol) in anhydrous THF (100 mL) *n*-BuLi (31.5 mL, 74.02 mmol, 2.5 M in hexane) was added under argon at -78ºC. Next, the cooling dry ice-acetone bath was removed, the mixture was allowed to warm up to -20ºC and then it was again cooled to -78ºC by dry ice bath. The acetal **5** (17.00 g, 71.05 mmol) solution in THF (50 mL) was then added dropwise, keeping the solution temperature below -55ºC. After addition of **5**, the mixture was stirred at -78ºC for 2h. The iodine (22.0 g, 85.26 mmol) solution in THF (50 mL) was then added by fast injection. Then the cooling bath was removed, and the mixture was allowed to reach room temperature. Ethyl acetate was then added, and the mixture was washed with sodium sulfite. The phases were separated, and the organic phase was concentrated, giving

a crude product. The product was then subjected to the column chromatography (ethyl acetate:hexane 1:15, SiO_2). The isolated product was then dissolved in homogenous mixture of THF/MeOH/H_2O and a few drops of HCl (37%) were added. The progress of the deprotection of formyl group was monitored by TLC (ethyl acetate: hexane 1:10, SiO_2). Upon reaction completion, sodium carbonate water solution was added, and the organic solvents were removed under reduced pressure. Then, the product was extracted with ethyl acetate, the phases were separated, dried with Na_2SO_4, and evaporated, giving the product as a brown oil which crystalized overnight. The product was obtained with 40 % yield (9.00 g, 28.93 mmol). ^{1}H NMR (400 MHz, $CDCl_3$) δ 9.72 (s, 1H), 6.99 (d, J = 3.9 Hz, 1H), 6.60 (d, J = 3.9 Hz, 1H), 1.69 (s, 9H). HR-MS (ESI+) *m/z* $[M+Na]^+$ 343.9740, calculated for: $C_{10}H_{12}NO_3INa^+$ 343.9760.

5-(furan-2-yl)-N-t-butoxycarbonyl-pyrrole-2-carbaldehyde (7) To the mixture of THF (100 mL) and water (3 mL) **5** (3.7 g, 11.9 mmol), 2-furanylboronic acid **2** (1.73 g, 15.46 mmol), palladium (0) tetrakis triphenylphosphine (0.7 g, 0.6 mmol), sodium carbonate (3.78 g, 35.7 mmol) and tetra-*n*- butylammonium chloride (1.3 g, 11.9 mmol) were added. The mixture was then degassed by a few vacuum-argon cycles and refluxed for 4 h. After that time the organic solvent was removed under reduced pressure and ethyl acetate was added to the residue. The water phase was extracted. The collected organic phase was washed with brine, dried over $MgSO_4$, and the solvent was removed under reduced pressure. The residue was then dissolved in THF (100 mL) and DMAP 4-dimethylaminopyridine, (0.3 g, 2.4 mmol) and di-*t*-butyl dicarbonate (2.73 g, 11.9 mmol) and triethylamine (10 mL) were added. The mixture was stirred for 30 min and water (10 mL) was added. The mixture was then stirred for additional 30 min. Next, the mixture was processed with a standard workup and the product was isolated by column chromatography (hexane:ethyl acetate 20:1→10:1, SiO_2) with 65% yield (2.02 g, 7.73 mmol) as a yellow oil. The compound was used in the next step of synthesis directly after its isolation.

N,N'-di-*t*-butoxycarbonyl-α,ω-dialdehyde (8) To the compound **7** (1.77 g, 6.77 mmol) and **1** (2.74 g, 6.77 mmol) dissolved in methylene chloride (150 mL) under argon $BF_3 \cdot Et_2O$ (1.00 ml; 8.12 mmol) was added. The reaction was stirred for 5 min, and after that time, the mixture was washed with sodium carbonate water solution. Next, the mixture was subjected to standard workup and the product was isolated by column chromatography (hexane:ethyl acetate 1:5, SiO_2) with 55% yield as a pale yellow solid (2.41 g, 3.72 mmol). ^{1}H NMR (400 MHz, $CDCl_3$) δ 9.99 (s, 1H), 9.77 (s, 1H), 7.04 (d, J = 2.7 Hz, 1H), 7.03 (d, J = 2.9 Hz, 1H), 6.63 (d, J = 3.3 Hz, 1H), 6.49 (d, J = 3.9 Hz, 1H), 6.03 (d, J = 3.3 Hz, 1H), 5.94 (d, J = 3.3 Hz, 1H), 5.86 (d, J = 3.7 Hz, 1H), 5.80 (d, J = 3.3 Hz, 1H), 4.37 (s, 2H), 4.25 (s, 2H), 1.59 (s, 9H), 1.57 (s, 8H), 1.39 (s, 9H). ^{13}C NMR (101 MHz, $CDCl_3$) δ 180.64, 179.00, 154.97, 149.65, 149.16, 149.02, 143.53, 141.63, 134.92, 133.95, 131.88, 131.71, 130.79, 121.77, 121.27, 112.13, 111.92, 111.57, 111.25, 111.06, 108.17, 86.06, 85.81, 84.29, 30.08, 29.07, 27.73, 27.65, 27.42. MS (EI+) found *m/z* $[M+Na]^+$ 670,27, calculated for $C_{35}H_{41}N_3NaO_9^+$670.2729

α,ω-dialdehyde (9) The compound was synthesized by the deprotection of NH groups in hot DMF (35 mL), analogically to previously reported deprotection procedure [3, 8]. The substrate **8** (1.24 g, 2.07 mmol) gave dialdehyde **9** (0.66 g, 1.90 mmol) as a pale brown solid with 92%

yield. ^{1}H NMR (400 MHz, DMSO-d$_6$) δ 12.37 (s, 1H), 11.92 (s, 1H), 10.59 (s, 1H), 9.45 (s, 1H), 9.34 (s, 1H), 7.04 (s, 1H), 6.95 (s, 1H), 6.88 (s, 1H), 6.50 (s, 1H), 6.19 (s, 1H), 6.02 (s, 1H), 5.71 (s, 1H), 5.68 (s, 1H), 3.92 (s, 2H), 3.85 (s, 2H). ^{13}C NMR (101 MHz, DMSO) δ 179.04, 178.57, 154.70, 145.47, 141.28, 133.50, 132.35, 131.78, 127.94, 126.55, 109.73, 108.61, 108.54, 107.76, 106.21, 106.13, 26.95, 26.33. HR-MS (ESI+) *m/z* found $[M+Na]^+$ 370.1158, calculated for $C_{20}H_{17}N_3O_3Na^+$ 370.1168.

22-oxahemiporphycene (22-O-HPc) To the suspension of zinc dust (9.035 g, 139 mmol), copper (I) chloride (0.6 g, 6.0 mmol) in THF (200 mL) under argon and cooled by ice bath, titanium (IV) chloride (7.63 mL, 69.5 mmol) was added. Next, the mixture was refluxed for 1 h. After that time the mixture was cooled to room temperature and **9** (483 mg, 1.39 mmol) was added in THF (20 mL). The reaction was carried out for 10 min and after that the mixture was cooled to 0ºC. Ammonia (25%, 25 mL) was then slowly added, maintaining the temperature below 10ºC. Further workup and oxidation with iodide were analogous to a previously reported procedure [8]. The product was obtained as a deep-violet solid with 11.5% yield (50 mg, 0.16 mmol). ^{1}H NMR (600 MHz, TFA-d) δ 11.64 (s, 1H), 11.43 (s, 1H), 11.08 (s, 2H), 11.06 (d, *J* = 4.7 Hz, 1H), 10.84 (d, *J* = 4.7 Hz, 1H), 10.50 (d, *J* = 4.7 Hz, 1H), 10.19 (d, *J* = 4.5 Hz, 1H), 10.15 (d, *J* = 4.7 Hz, 1H), 10.12 (d, *J* = 4.7 Hz, 1H), 9.95 (d, *J* = 4.7 Hz, 1H), 9.94 (d, *J* = 4.6 Hz, 1H). ^{13}C NMR (151 MHz, TFA-d) δ 153.69, 149.29, 148.67, 144.11, 143.96, 141.73, 141.56, 135.72, 135.29, 133.90, 133.56, 133.08, 132.67, 131.74, 127.76, 127.46, 120.68, 117.63, 111.85, 107.07. HR-MS (ESI+) *m/z* $[M+H]^+$ found 312.1124, calculated for $C_{20}H_{14}N_3O^+$ 312.1137.

14. References

[1] Y. Yuzhelevski, M. Yuzhelevski, G. Jung, Random telegraph noise analysis in time domain, Rev. Sci. Instr., 71 (2000) 1681-1688.
[2] E. Durant, PhD Thesis, University of Liverpool, UK, DOI (2021).
[3] J. Ostapko, K. Nawara, M. Kijak, J. Buczynska, B. Lesniewska, M. Pietrzak, G. Orzanowska, J. Waluk, Parent, unsubstituted hemiporphycene: synthesis and properties, Chem. Eur. J., 22 (2016) 17311-17320.
[4] D.M. Knapp, E.P. Gillis, M.D. Burke, A General Solution for Unstable Boronic Acids: Slow-Release Cross-Coupling from Air-Stable MIDA Boronates, J. Am. Chem. Soc., 131 (2009) 6961-6963.
[5] Y. He, M. Lin, Z. Li, X. Liang, G. Li, J.C. Antilla, Direct Synthesis of Chiral 1,2,3,4-Tetrahydropyrrolo[1,2- a]Pyrazines via a Catalytic Asymmetric Intramolecular Aza-Friedel–Crafts Reaction, Org. Lett., 13 (2011) 4490-4493.
[6] J. Waser, B. Gaspar, H. Nambu, E.M. Carreira, Hydrazines and Azides via the Metal-Catalyzed Hydrohydrazination and Hydroazidation of Olefins, J. Am. Chem. Soc., 128 (2006) 11693-11712.
[7] C.-Y. Chen, D.F. Bocian, J.S. Lindsay, Synthesis of 24 Bacteriochlorin Isotopologues, Each Containing a Symmetrical Pair of 13 C or 15 N Atoms in the Inner Core of the Macrocycle, J. Org. Chem., 79 (2014) 1001-1016.
[8] J. Ostapko, A. Kelm, M. Kijak, B. Lesniewska, J. Waluk, Two macrocycles in one shot: synthesis, spectroscopy, photophysics, and tautomerism of 23-oxahemiporphycene and 21-oxacorrole-5-carbaldehyde, Chem. Eur. J., 24 (2018) 9884-9891.